Inclusive production of charged pions, charged and neutral kaons and antiprotons in $e^+ e^-$ annihilation at 10 GeV and in direct Upsilon decays

ARGUS Collaboration

H. Albrecht, P. Böckmann, R. Gläser, G. Harder,
A. Krüger, A. Nippe, M. Reidenbach, M. Schäfer,
W. Schmidt-Parzefall, H. Schröder, H.D. Schulz,
F. Sefkow, J. Spengler, R. Wurth, A. Yagil

DESY, D-2000 Hamburg, Federal Republic of Germany

R.D. Appuhn, A. Drescher, C. Hast, G. Herrera,
D. Kamp, H. Kolanoski, A. Lindner, R. Mankel,
H. Scheck, G. Schweda, B. Spaan, A. Walther,
D. Wegener

Institut für Physik[1], Universität, D-4600 Dortmund,
Federal Republic of Germany

W. Funk, J.C. Gabriel, J. Stiewe, S. Werner

Institut für Hochenergiephysik[2], Universität,
D-6900 Heidelberg, Federal Republic of Germany

K.W. Edwards[3], W.R. Frisken[4], H. Kapitza[3],
R. Kutschke[5], D.B. MacFarlane[6], K.W. McLean[6],
A.W. Nilsson[6], R.S. Orr[5], J.A. Parsons[5],
P.M. Patel[6], J.D. Prentice[5], S.C. Seidel[5],
J.D. Swain[5], G. Tsipolitis[6], T.-S. Yoon[5]

Institute of Particle Physics[7], Canada

R. Ammar, S. Ball, D. Coppage, R. Davis,
S. Kanekal, N. Kwak

University of Kansas[8], Lawrence, KS 66044, USA

T. Ruf, S. Schael, K.R. Schubert, K. Strahl, R. Waldi

Institut für Experimentelle Kernphysik[9], Universität,
D-7500 Karlsruhe, Federal Republic of Germany

B. Boštjančič, G. Kernel, P. Križan, E. Križnič,
M. Pleško

Institut J. Stefan and Oddelek za fiziko[10], Univerza v Ljubljani,
YU-61000 Ljubljana, Yugoslavia

H.I. Cronström, L. Jönsson

Institute of Physics[11], University of Lund, S-22362 Lund, Sweden

A. Babaev, M. Danilov, B. Fominykh, A. Golutvin,
I. Gorelov, V. Lubimov, A. Rostovtsev, A. Semenov,
S. Semenov, V. Shevchenko, V. Soloshenko,
V. Tchistilin, I. Tichomirov, Yu. Zaitsev

Institute of Theoretical and Experimental Physics,
SU-117259 Moscow, USSR

R. Childers, C.W. Darden, R.C. Fernholz

University of South Carolina[12], Columbia, SC 29208, USA

Abstract. Using the ARGUS detector at the e^+e^- storage ring DORIS II, we have investigated inclusive production of $\pi^\pm, K^\pm, K_s^0$ and $\bar{p}$ in multihadron events at 9.98 GeV and in direct decays of the $\Upsilon(1S)$ meson, i.e. from quark and gluon fragmentation. The most pronounced difference is the rate of baryon production. The Lund Monte Carlo program gives a reasonable qualitative description, although it cannot reproduce our data in detail.

Multihadron final states in e^+e^- annihilation are produced via quark and antiquark fragmentation, those from direct $\Upsilon(1S)$ decays originate from the hadronization of three gluons. Data from these processes allow a test of our present ideas on quark and gluon fragmentation. One of the most striking differences observed so far [1–3] is the rate of baryon production. Many alternative explanations have been proposed [4], and more precise data are needed to improve our understanding of this phenomenon. In this paper, we present a study of inclusive production of protons as well as charged pions and charged and neutral kaons, which as final products of the fragmentation and decay chain give information on the global properties of the hadronization of quarks and gluons.

The data used for this analysis have been collected in 1983 with the ARGUS detector [5] at the e^+e^- storage ring DORIS II at DESY, and comprise an integrated luminosity of 6.6/pb at the $\Upsilon(1S)$ energy and 2.6/pb in the nearby continuum. For this data taking period, the drift chamber performance, which plays an important role for charged particle identification, has been studied in great detail.

Multihadron final states were selected by requiring at least four charged tracks from the interaction region, and a total energy deposition of more than 1.7 GeV in the shower counters. These cuts almost completely eliminate contributions from muon pair production, photon-photon annihilation, beam gas and beam wall interactions. In addition, we reject events containing at least two tracks with $p > 2.5$ GeV/c and an energy $E_{sh} > 1.5$ GeV deposited in the shower counters, to discard the remaining background from radiative Bhabha events, where a photon has converted into an e^+e^- pair.

After these cuts we are left with 9616 events in the continuum, and 82657 events on the $\Upsilon(1S)$ resonance. From these events, charged tracks were selected, which originate within 1.5 cm radially and 5 cm along the beam direction of the nominal interaction point. The momentum vector had to fulfill $p_\perp > 0.05$ GeV/c and $|\cos\theta| < 0.85$, both with respect to the beam axis, and we required 17 or more wires hit in the main drift chamber.

Charged particles can be identified using information from two detector components: the main drift chamber, providing dE/dx information, and the time-of-flight (TOF) counters, which surround the drift chamber at a radial distance of 95 cm from the interaction point.

The dE/dx samples from all hit wires are corrected for space charge effects and averaged, discarding the highest 30% and lowest 10% of the values [6]. The track cuts ensure that at least 10 hits contribute to this truncated mean.
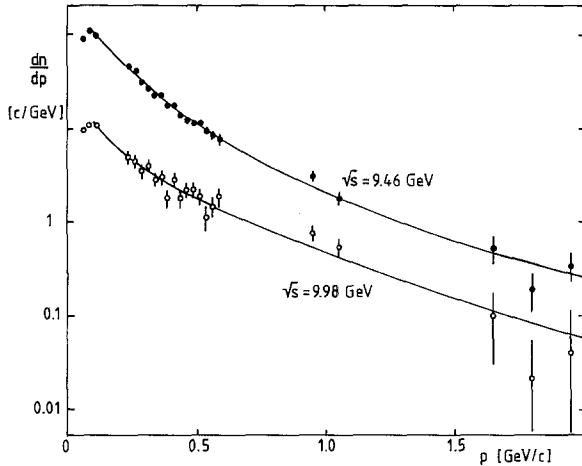
The time of flight is corrected for a pulse height dependent time shift [7]. It is only used as additional information for tracks with $|\cos\theta| < 0.60$, if a TOF counter can be uniquely assigned to the track.

Distributions in the specific energy loss, $f_j(dE/dx|\mathbf{p})$, and time of flight, $g_j(\text{TOF}|\mathbf{p})$, have been precisely parametrized for the selected data, using clean samples of electrons (from radiative Bhabha events), pions (from K_s^0 decays) and protons (from Λ decays), in the accessible range of momentum p and polar angle θ. The spectra for charged pions, kaons and antiprotons are obtained from a maximum likelihood fit of a sum of these distributions to all selected tracks, using as free parameters the numbers of $\pi^\pm, K^\pm, p+\bar{p}, e^\pm$ and $\mu^\pm$ in each momentum (or energy) bin [8]. The numbers of electrons and muons are further constrained to fit predetermined distributions $h_e(p)$ and $h_\mu(p)$. For electrons, h_e is a smooth function which is obtained from data in the regions where they can be well identified, as shown in Fig. 1. The distribution h_μ has been determined from the Lund Monte Carlo program [9], which gives predictions consistent with the number of observed muons at momenta above 1.4 GeV/c, where identification is made using the ARGUS muon chambers.

The complete likelihood function to be maximized for each momentum interval of charged tracks thus becomes

$$
\begin{aligned}
&L(n_\pi, n_K, n_p, n_e, n_\mu) \\
&= \prod_{i=1}^{N} \left(\sum_{j=\pi,K,p,e,\mu} \frac{n_j}{\sum n_k} \cdot f_j(\langle dE/dx \rangle_i|\mathbf{p}_i) \cdot g_j(\text{TOF}_i|\mathbf{p}_i) \right) \\
&\quad \cdot \exp\left(-\frac{[n_\mu - h_\mu(p)]^2}{2\sigma_\mu^2(p)} - \frac{[n_e - h_e(p)]^2}{2\sigma_e^2(p)} \right) \\
&\quad \cdot \exp\left(-\sum n_k \right) \cdot \left(\sum n_k \right)^N
\end{aligned} \tag{1}
$$

where p_i is the momentum measured in the drift chamber, N is the total number of observed charged tracks in the momentum interval, and the n_j are the numbers of particles of type j to be fitted. The third line of the likelihood function (1) reflects the Poisson

Fig. 1. Fit results and interpolation function for the absolute number of electrons. To account for electrons in the charged hadron data in momentum regions, where they can't be separated, their contribution is constrained to fit this interpolation function

Fig. 2 a, b. Illustration of the statistical particle separation. **a** The dE/dx distribution is shown together with the results of a fit for $0.65\ \mathrm{GeV/c} < p < 0.675\ \mathrm{GeV/c}$ Protons are still clearly separated in this momentum region. The pion area contains also all muons. **b** The time-of-flight distribution for the same momentum interval. Here electrons and muons are included in the "pion" contribution

distribution of the total number of tracks. This fit is performed in small intervals of the momentum at the interaction point for each hadron separately. In Fig. 2 we have superimposed the results of the fit to the observed dE/dx and TOF distributions in one interval for illustration.
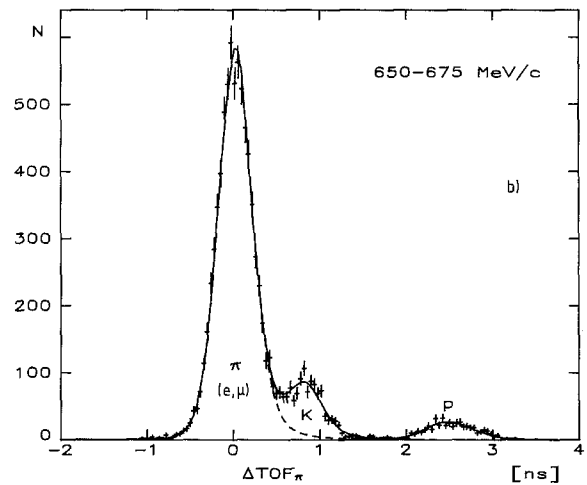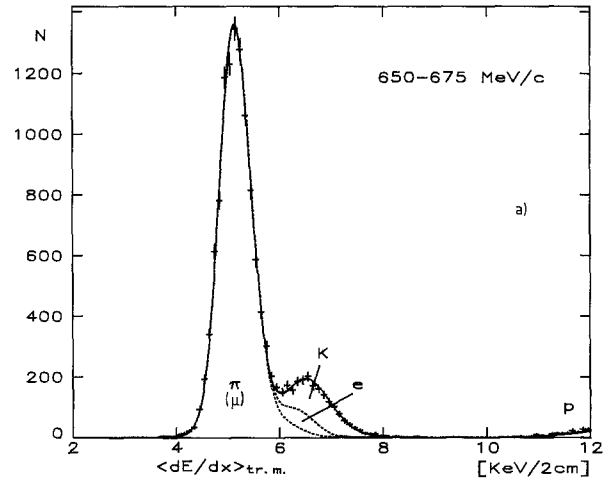
Since the acceptance for tracks from secondary vertices is different from that for tracks from the interaction region, the decay products of K_s^0 and Λ were treated separately*: Using momentum distributions of K^0 mesons (see below) and Λ baryons [3] obtained from the same experiment, we subtract all pions and (anti-) protons from the decays of these particles, which have not already been removed by the cut on the track origin.

K_s^0 mesons were selected [10] requiring a secondary vertex with two oppositely charged tracks, separated by at least 2 cm from the interaction point. The charged tracks had to be compatible with the pion hypothesis, $L_\pi > 0.09$, with the normalized likelihood

$$L_\pi = \frac{g_\pi e^{-(\chi^2_{TOF} + \chi^2_{dE/dx})_\pi/2}}{\sum\limits_{i=e,\mu,\pi,K,p} g_i e^{-(\chi^2_{TOF} + \chi^2_{dE/dx})_i/2}}$$

calculated from a priori particle frequencies g_i and dE/dx and TOF information. Furthermore, these tracks must have $p_\perp > 0.08$ GeV/c $|\cos\theta| < 0.9$ with respect to the beam axis. Furthermore, the angle ω be-

tween the momentum of the K_s^0 and its direction of flight, determined as the vector from the primary vertex to its decay vertex, had to be small, $\cos\omega > 0.9$, and the angle between the momenta of any pion candidate and the K_s^0 had to fulfill $|\cos\theta_{K,\pi}| < 0.98$ to reject converted photons. The K_s^0 signal obtained with these cuts is shown in Fig. 3.

The number of K_s^0 mesons is determined from a fit of the data in each momentum or energy bin to a linear background plus a signal with a shape determined by our resolution. This shape can be satisfactorily described by a sum of two Gaussians, with momentum dependent widths and composition. The fit function applied thus becomes

---

* The rare pions from charged kaon decay are removed implicitly within our acceptance correction. Subtracting – instead of adding – the weak K_s^0 and Λ decay products, seems to us more natural, since we thus remove the most trivial correlation between pion and kaon or lambda and proton production, respectively
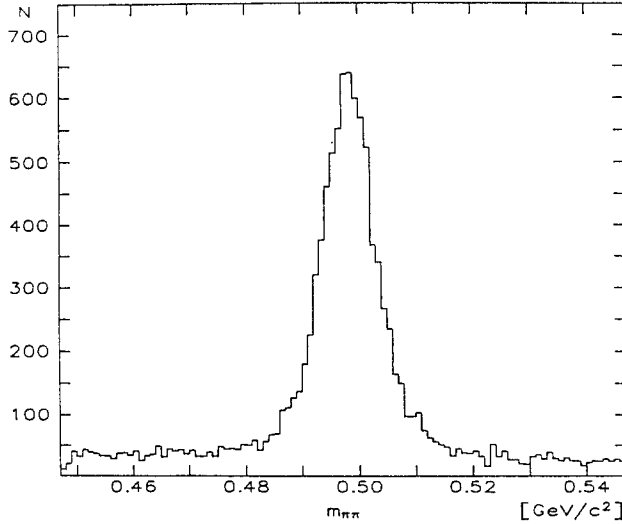
Fig. 3. K_s^0 signal at the $\Upsilon(1S)$ resonance energy

$$\phi_i(m) = a_i + b_i \cdot m + n_i \left(\frac{1}{\sqrt{2\pi}\sigma} e^{-(m-m_K)^2/2\sigma^2} \right.$$

$$\left. + \frac{A+B \cdot p^2}{\sqrt{2\pi}\sigma'} e^{-(m-m_K)^2/2\sigma'^2} \right)$$

where $\sigma = \sigma(p)$ is parametrized by a second order polynomial in p and $\sigma' = \sigma + C$. This fit is performed for all bins simultaneously, using six free global parameters* in addition to the a_i, b_i and n_i for each bin.

Misidentified Λ hyperons occurring at high momenta have been determined to contribute less than 2% to the K_s^0 signal in each momentum bin, and have been subtracted using Monte Carlo events.

All spectra in the continuum are corrected for contributions from the process $e^+ e^- \to \tau^+ \tau^-$ (γ), which constitutes a 4.8% fraction of the data after the cuts. The small amount of direct $\Upsilon(1S)$ decays from the radiative tail of the resonance curve, contributing 1.1% to the events at 9.98 GeV, is subtracted accordingly, using on-resonance data, whereas other radiative corrections have been applied using the Lund Monte Carlo program as described below.

To obtain particle spectra from direct $\Upsilon(1S)$ decays, the underlying continuum, as well as electromagnetic decays of the $\Upsilon(1S)$ to $q\bar{q}$ (and $\tau^+\tau^-$), have to be subtracted. Thus:

$$\frac{1}{\sigma_{dir}} \frac{d\sigma_{dir}(p)}{dp} = a \cdot \frac{1}{\sigma_{on}} \frac{d\sigma_{on}(p)}{dp} - a' \cdot \frac{1}{\sigma_{off}} \frac{d\sigma_{off}(p)}{dp}$$

$$- a'' \cdot \frac{1}{\sigma_{vp}} \frac{d\sigma_{vp}(p)}{dp} \qquad (2)$$

---

* A, B, C and the three coefficients of the $\sigma(p)$ parametrization

where the subscript "dir" refers to direct decays, "on" to all hadronic events on the $\Upsilon(1S)$ resonance, "off" to all events in the continuum after removing contributions from $e^+ e^- \to \gamma \Upsilon(1S)$, and "vp" (vacuum polarisation) to events from the electromagnetic decays of the $\Upsilon(1S)$, which can be obtained from the continuum data after radiative correction. The last term also includes a small fraction of $\Upsilon(1S) \to \tau^+ \tau^-$. Using $\sigma_{cont} = \sigma_{off} \cdot s_{off}/s_{on}$ and $\sigma_\Upsilon = \sigma_{on} - \sigma_{cont}$, we obtain

$$\sigma_{vp} = \sigma_\Upsilon \cdot (R + f_\tau) \cdot BR(\Upsilon(1S) \to \mu^+ \mu^-)$$
$$\sigma_{dir} = \sigma_\Upsilon - \sigma_{vp}$$
$$a = \sigma_{on}/\sigma_{dir}$$
$$a' = \sigma_{cont}/\sigma_{dir}$$
$$a'' = \sigma_{vp}/\sigma_{dir}$$

where f_τ is the fraction of tau pair events with at least four charged particles, and all cross sections are understood to include only hadronic final states.

In order to calculate the acceptance, and correct the continuum data to the lowest order QED process $e^+ e^- \to q\bar{q}$, events were simulated using the Lund Monte Carlo program (version 6.2 [9]). Direct $\Upsilon(1S)$ decays are modelled by the three gluon and $\gamma g g$ decay routines. For $e^+ e^- \to q\bar{q}(\gamma)$ events, the original program has been slightly modified to include the contribution of vector meson resonances to the initial-photon spectrum [11]. All events were subsequently passed through a simulation of the ARGUS detector [12], and processed with the same reconstruction and analysis programs as the data.

The angular distribution of charged particles in the continuum was found to be significantly different
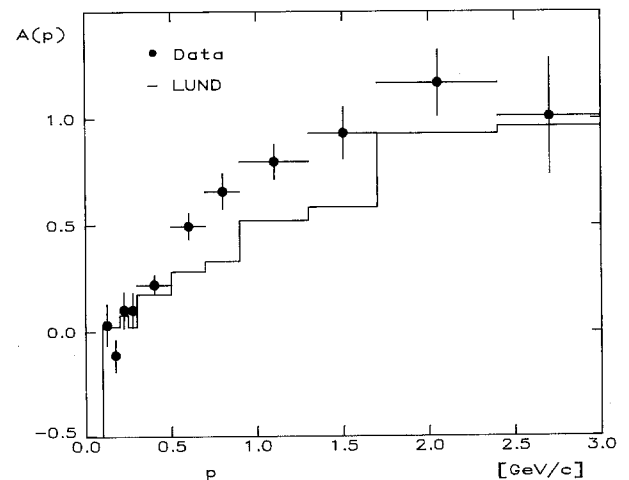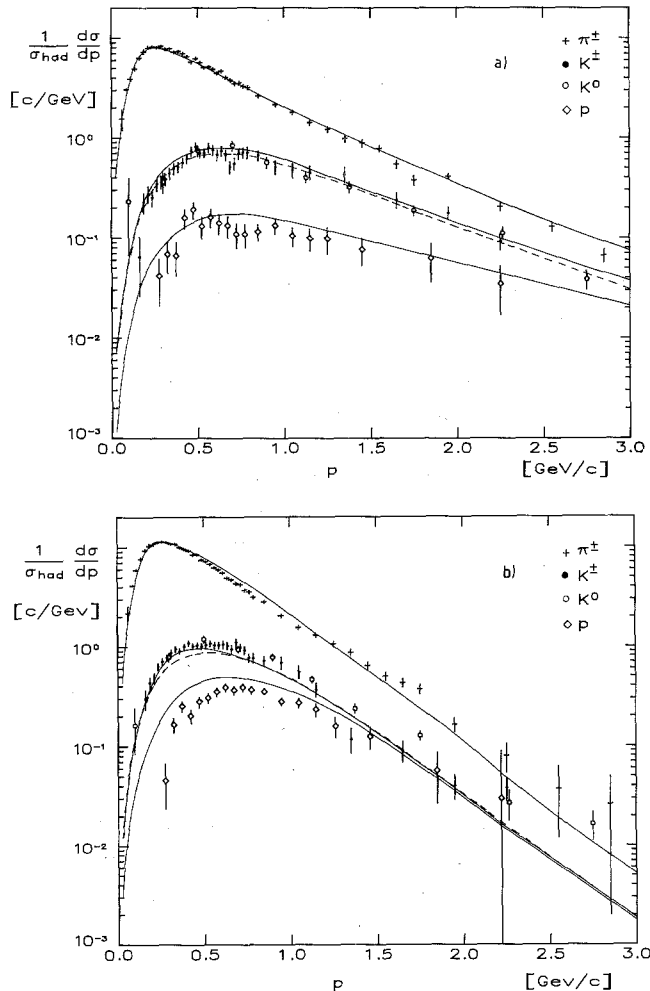

Fig. 4. Parameter $A(p)$ of the polar angle distribution for charged hadrons in $e^+ e^-$ annihilation events at 9.98 GeV, as obtained from a fit of uncorrected data to $dn/d\cos\theta \propto 1 + A(p)\cos^2\theta$ in the range $|\cos\theta| < 0.75$. The solid histogram is the result of the Lund Monte Carlo program

from our data, as shown in Fig. 4. We investigated two possible sources of this discrepancy: Changing α_s within a reasonable range, 0.17 to 0.25, did not give any significant changes in the inclusive angular distribution. Therefore we exclude an overestimation of gluon radiation as a possible source. Changing the width of the transverse momentum distribution of the primary hadrons with respect to the parton axis does alter Fig. 4. However, only a reduction of $\sigma_\perp$ to zero, i.e. producing no $p_\perp$ at all, could give approximate agreement. So we did not tune the Monte Carlo program, but corrected the acceptance function for the discrepancy.

The resulting momentum spectra are shown in Fig. 5a for quark fragmentation from $e^+e^- \to q\bar{q}$ and

in Fig. 5b for gluon fragmentation from decays $\Upsilon(1S) \to ggg, \gamma gg$. In all distributions, instead of $p+\bar{p}$, two times the number of antiprotons is shown, in order to avoid any problems with protons which originate from secondary interactions or the small amount of remaining beam-gas events. The spectra are listed numerically in Tables 1–4.

The normalized scaling cross sections

$$\frac{1}{\sigma_{\text{had}}} \frac{d\sigma}{\beta \, dz} = \frac{1}{n_{\text{ev}}} \frac{dn}{\eta(z) \beta \, dz}$$

are shown in Figs. 6 and 7 and tabulated in Tables 5–8. The variable $z = 2E/\sqrt{s}$ is the scaled particle energy, n_{ev} the number of selected multihadron events, and $\eta(z)$ the acceptance function, which describes the efficiency to reconstruct and select a particle within these

Fig. 5. a Momentum distribution of $\pi^\pm, K^\pm, K^0/\bar{K}^0$ and $p/\bar{p}$ in $e^+e^- \to$ hadrons at 9.98 GeV ($\pi^\pm$ and protons from K_s^0 and Λ decays have been subtracted). The curve is the Lund prediction (solid = charged hadrons, dashed = K^0). **b** Momentum distribution of $\pi^\pm, K^\pm, K^0/\bar{K}^0$ and $p/\bar{p}$ in direct $\Upsilon(1S)$ decays ($\pi^\pm$ and protons from K_s^0 and Λ decays have been subtracted). The curve is the Lund prediction (solid = charged hadrons, dashed = K^0)

Table 1. $\dfrac{1}{\sigma_{\text{had}}} \dfrac{d\sigma(\pi^\pm)}{dp}$ in c/GeV of direct $\Upsilon(1S)$ decays and of e^+e^--annihilation at 9.98 GeV. An overall uncertainty of $\pm 1.8\%$ is not included in the systematic errors

p interval	$\Upsilon(1S)_{\text{dir}}$	continuum at 9.98 GeV
0.050 − 0.075 GeV/c	2.165 ± 0.256 ± 0.259	1.544 ± 0.365 ± 0.019
0.075 − 0.100 GeV/c	4.118 ± 0.057 ± 0.013	3.059 ± 0.066 ± 0.005
0.100 − 0.125 GeV/c	5.893 ± 0.158 ± 0.063	3.901 ± 0.164 ± 0.034
0.125 − 0.150 GeV/c	7.638 ± 0.172 ± 0.213	4.939 ± 0.176 ± 0.133
0.150 − 0.175 GeV/c	9.287 ± 0.193 ± 0.258	6.346 ± 0.200 ± 0.169
0.175 − 0.200 GeV/c	10.301 ± 0.207 ± 0.412	7.282 ± 0.217 ± 0.286
0.200 − 0.225 GeV/c	10.670 ± 0.216 ± 0.224	7.971 ± 0.230 ± 0.154
0.225 − 0.250 GeV/c	11.073 ± 0.213 ± 0.100	8.102 ± 0.231 ± 0.031
0.250 − 0.275 GeV/c	11.264 ± 0.216 ± 0.098	7.985 ± 0.228 ± 0.026
0.275 − 0.300 GeV/c	11.117 ± 0.214 ± 0.103	8.292 ± 0.230 ± 0.038
0.300 − 0.325 GeV/c	10.731 ± 0.206 ± 0.110	7.744 ± 0.223 ± 0.049
0.325 − 0.350 GeV/c	10.688 ± 0.205 ± 0.098	7.809 ± 0.224 ± 0.037
0.350 − 0.375 GeV/c	9.899 ± 0.199 ± 0.099	7.217 ± 0.213 ± 0.045
0.375 − 0.400 GeV/c	9.541 ± 0.197 ± 0.091	7.333 ± 0.215 ± 0.041
0.400 − 0.425 GeV/c	9.156 ± 0.190 ± 0.091	6.965 ± 0.210 ± 0.045
0.425 − 0.450 GeV/c	8.355 ± 0.183 ± 0.077	6.521 ± 0.201 ± 0.034
0.450 − 0.475 GeV/c	8.409 ± 0.177 ± 0.074	5.761 ± 0.183 ± 0.028
0.475 − 0.500 GeV/c	7.378 ± 0.175 ± 0.069	6.168 ± 0.188 ± 0.037
0.500 − 0.525 GeV/c	7.107 ± 0.169 ± 0.061	5.611 ± 0.180 ± 0.027
0.525 − 0.550 GeV/c	6.674 ± 0.160 ± 0.054	5.016 ± 0.171 ± 0.023
0.550 − 0.575 GeV/c	6.174 ± 0.153 ± 0.050	5.103 ± 0.171 ± 0.023
0.575 − 0.600 GeV/c	5.897 ± 0.149 ± 0.049	4.830 ± 0.167 ± 0.026
0.600 − 0.625 GeV/c	5.481 ± 0.143 ± 0.042	4.431 ± 0.161 ± 0.021
0.625 − 0.650 GeV/c	4.865 ± 0.142 ± 0.040	4.677 ± 0.164 ± 0.025
0.650 − 0.675 GeV/c	4.677 ± 0.135 ± 0.040	4.027 ± 0.154 ± 0.026
0.675 − 0.700 GeV/c	4.282 ± 0.131 ± 0.045	3.780 ± 0.150 ± 0.034
0.700 − 0.725 GeV/c	4.180 ± 0.126 ± 0.047	3.484 ± 0.144 ± 0.035
0.725 − 0.750 GeV/c	3.674 ± 0.125 ± 0.047	3.503 ± 0.146 ± 0.041
0.750 − 0.775 GeV/c	3.503 ± 0.121 ± 0.048	3.240 ± 0.139 ± 0.043
0.775 − 0.800 GeV/c	3.109 ± 0.119 ± 0.058	3.159 ± 0.140 ± 0.057
0.800 − 0.900 GeV/c	2.804 ± 0.057 ± 0.076	2.605 ± 0.067 ± 0.070
0.900 − 1.000 GeV/c	2.032 ± 0.055 ± 0.065	2.139 ± 0.065 ± 0.068
1.000 − 1.100 GeV/c	1.540 ± 0.057 ± 0.049	1.777 ± 0.069 ± 0.056
1.100 − 1.200 GeV/c	1.290 ± 0.060 ± 0.031	1.411 ± 0.075 ± 0.032
1.200 − 1.300 GeV/c	1.057 ± 0.056 ± 0.038	1.208 ± 0.070 ± 0.042
1.300 − 1.400 GeV/c	0.858 ± 0.050 ± 0.047	0.971 ± 0.063 ± 0.051
1.400 − 1.500 GeV/c	0.634 ± 0.044 ± 0.039	0.876 ± 0.057 ± 0.050
1.500 − 1.600 GeV/c	0.491 ± 0.038 ± 0.025	0.765 ± 0.049 ± 0.028
1.600 − 1.700 GeV/c	0.425 ± 0.033 ± 0.023	0.535 ± 0.043 ± 0.019
1.700 − 1.800 GeV/c	0.370 ± 0.031 ± 0.023	0.373 ± 0.040 ± 0.013
1.800 − 1.900 GeV/c	0.165 ± 0.030 ± 0.021	0.536 ± 0.041 ± 0.017
1.900 − 2.000 GeV/c	0.174 ± 0.027 ± 0.021	0.385 ± 0.036 ± 0.012
2.000 − 2.100 GeV/c	0.148 ± 0.024 ± 0.022	0.292 ± 0.033 ± 0.014
2.100 − 2.200 GeV/c	0.119 ± 0.021 ± 0.022	0.189 ± 0.029 ± 0.008
2.200 − 2.300 GeV/c	0.057 ± 0.021 ± 0.022	0.241 ± 0.030 ± 0.010
2.300 − 2.400 GeV/c	0.062 ± 0.018 ± 0.022	0.176 ± 0.026 ± 0.007
2.400 − 2.500 GeV/c	0.053 ± 0.016 ± 0.023	0.123 ± 0.023 ± 0.007
2.500 − 2.600 GeV/c	0.010 ± 0.014 ± 0.023	0.159 ± 0.021 ± 0.008
2.600 − 2.700 GeV/c	0.049 ± 0.014 ± 0.023	0.102 ± 0.020 ± 0.006
2.700 − 2.800 GeV/c	0.046 ± 0.011 ± 0.023	0.061 ± 0.016 ± 0.004
2.800 − 2.900 GeV/c	0.013 ± 0.011 ± 0.023	0.090 ± 0.017 ± 0.003
2.900 − 3.000 GeV/c	0.019 ± 0.010 ± 0.023	0.048 ± 0.015 ± 0.006

Table 2. $\dfrac{1}{\sigma_{\text{had}}}\dfrac{d\sigma(K^{\pm})}{dp}$ in c/GeV of direct $\Upsilon(1S)$ decays and of e^+e^--annihilation at 9.98 GeV. An overall uncertainty of $\pm 1.8\%$ is not included in the systematic errors

p interval	$\Upsilon(1S)_{\text{dir}}$	continuum at 9.98 GeV
0.150 − 0.175 GeV/c	0.299 ± 0.064 ± 0.013	0.064 ± 0.038 ± 0.002
0.175 − 0.200 GeV/c	0.433 ± 0.053 ± 0.003	0.227 ± 0.050 ± 0.001
0.200 − 0.225 GeV/c	0.492 ± 0.049 ± 0.002	0.274 ± 0.051 ± 0.001
0.225 − 0.250 GeV/c	0.627 ± 0.048 ± 0.004	0.248 ± 0.045 ± 0.001
0.250 − 0.275 GeV/c	0.707 ± 0.053 ± 0.004	0.342 ± 0.051 ± 0.001
0.275 − 0.300 GeV/c	0.776 ± 0.053 ± 0.004	0.359 ± 0.052 ± 0.001
0.300 − 0.325 GeV/c	0.872 ± 0.054 ± 0.005	0.384 ± 0.052 ± 0.001
0.325 − 0.350 GeV/c	0.950 ± 0.059 ± 0.006	0.437 ± 0.055 ± 0.001
0.350 − 0.375 GeV/c	0.907 ± 0.057 ± 0.005	0.488 ± 0.059 ± 0.001
0.375 − 0.400 GeV/c	1.006 ± 0.058 ± 0.007	0.508 ± 0.059 ± 0.001
0.400 − 0.425 GeV/c	1.089 ± 0.061 ± 0.009	0.563 ± 0.062 ± 0.003
0.425 − 0.450 GeV/c	1.015 ± 0.063 ± 0.009	0.617 ± 0.064 ± 0.004
0.450 − 0.475 GeV/c	1.038 ± 0.065 ± 0.010	0.738 ± 0.072 ± 0.006
0.475 − 0.500 GeV/c	1.002 ± 0.066 ± 0.012	0.803 ± 0.074 ± 0.008
0.500 − 0.525 GeV/c	1.036 ± 0.062 ± 0.017	0.690 ± 0.068 ± 0.010
0.525 − 0.550 GeV/c	1.073 ± 0.066 ± 0.027	0.698 ± 0.069 ± 0.017
0.550 − 0.575 GeV/c	1.031 ± 0.066 ± 0.042	0.793 ± 0.077 ± 0.032
0.575 − 0.600 GeV/c	1.031 ± 0.064 ± 0.048	0.749 ± 0.075 ± 0.035
0.600 − 0.625 GeV/c	1.046 ± 0.066 ± 0.061	0.669 ± 0.071 ± 0.039
0.625 − 0.650 GeV/c	1.021 ± 0.068 ± 0.051	0.735 ± 0.075 ± 0.036
0.650 − 0.675 GeV/c	0.939 ± 0.065 ± 0.056	0.669 ± 0.067 ± 0.039
0.675 − 0.700 GeV/c	1.099 ± 0.066 ± 0.076	0.504 ± 0.062 ± 0.034
0.700 − 0.725 GeV/c	0.981 ± 0.062 ± 0.058	0.546 ± 0.066 ± 0.032
0.725 − 0.750 GeV/c	0.922 ± 0.065 ± 0.052	0.694 ± 0.072 ± 0.038
0.750 − 0.775 GeV/c	0.759 ± 0.066 ± 0.036	0.699 ± 0.073 ± 0.032
0.775 − 0.800 GeV/c	0.763 ± 0.068 ± 0.057	0.699 ± 0.076 ± 0.051
0.800 − 0.900 GeV/c	0.715 ± 0.036 ± 0.071	0.658 ± 0.041 ± 0.064
0.900 − 1.000 GeV/c	0.683 ± 0.039 ± 0.088	0.504 ± 0.044 ± 0.064
1.000 − 1.100 GeV/c	0.551 ± 0.048 ± 0.065	0.467 ± 0.055 ± 0.054
1.100 − 1.200 GeV/c	0.365 ± 0.054 ± 0.021	0.445 ± 0.064 ± 0.025
1.200 − 1.300 GeV/c	0.156 ± 0.051 ± 0.020	0.477 ± 0.062 ± 0.059
1.300 − 1.400 GeV/c	0.133 ± 0.045 ± 0.024	0.421 ± 0.055 ± 0.072
1.400 − 1.500 GeV/c	0.060 ± 0.038 ± 0.012	0.368 ± 0.048 ± 0.069
1.500 − 1.600 GeV/c	0.118 ± 0.030 ± 0.024	0.234 ± 0.036 ± 0.045
1.600 − 1.700 GeV/c	0.091 ± 0.025 ± 0.013	0.230 ± 0.031 ± 0.032
1.700 − 1.800 GeV/c	0.057 ± 0.023 ± 0.008	0.243 ± 0.029 ± 0.031
1.800 − 1.900 GeV/c	0.043 ± 0.020 ± 0.007	0.193 ± 0.026 ± 0.026
1.900 − 2.000 GeV/c	0.051 ± 0.019 ± 0.006	0.182 ± 0.024 ± 0.020
2.000 − 2.100 GeV/c	0.025 ± 0.017 ± 0.004	0.147 ± 0.022 ± 0.017
2.100 − 2.200 GeV/c	0.035 ± 0.017 ± 0.005	0.126 ± 0.022 ± 0.014
2.200 − 2.300 GeV/c	0.045 ± 0.016 ± 0.009	0.072 ± 0.021 ± 0.013
2.300 − 2.400 GeV/c	0.034 ± 0.016 ± 0.006	0.076 ± 0.021 ± 0.010

Table 3. $\dfrac{1}{\sigma_{\text{had}}}\dfrac{d\sigma(K^0/\bar{K}^0)}{dp}$ in c/GeV of direct $\Upsilon(1S)$ decays and of e^+e^--annihilation at 9.98 GeV. An overall systematic uncertainty of $\pm 3.6\%$ has to be added

p interval	$\Upsilon(1S)_{\text{dir}}$	continuum at 9.98 GeV
0.00 − 0.20 GeV/c	0.161 ± 0.077	0.228 ± 0.161
0.20 − 0.40 GeV/c	0.780 ± 0.076	0.359 ± 0.080
0.40 − 0.60 GeV/c	1.177 ± 0.087	0.734 ± 0.088
0.60 − 0.80 GeV/c	0.932 ± 0.067	0.834 ± 0.090
0.80 − 1.00 GeV/c	0.772 ± 0.061	0.560 ± 0.068
1.00 − 1.25 GeV/c	0.459 ± 0.035	0.393 ± 0.043
1.25 − 1.50 GeV/c	0.235 ± 0.024	0.317 ± 0.038
1.50 − 2.00 GeV/c	0.127 ± 0.014	0.186 ± 0.020
2.00 − 2.50 GeV/c	0.0268 ± 0.0089	0.111 ± 0.016
2.50 − 3.00 GeV/c	0.0164 ± 0.0052	0.0382 ± 0.0084

Table 4. $2\cdot\dfrac{1}{\sigma_{\text{had}}}\dfrac{d\sigma(\bar{p})}{dp}$ in c/GeV of direct $\Upsilon(1S)$ decays and of e^+e^--annihilation at 9.98 GeV. An overall uncertainty of $\pm 1.8\%$ is not included in the systematic errors

p interval	$\Upsilon(1S)_{\text{dir}}$	continuum at 9.98 GeV
0.250 − 0.300 GeV/c	0.0452 ± 0.0215 ± 0.0013	0.0409 ± 0.0203 ± 0.0002
0.300 − 0.350 GeV/c	0.1652 ± 0.0269 ± 0.0003	0.0677 ± 0.0235 ± 0.0002
0.350 − 0.400 GeV/c	0.2524 ± 0.0281 ± 0.0015	0.0656 ± 0.0244 ± 0.0002
0.400 − 0.450 GeV/c	0.2018 ± 0.0317 ± 0.0011	0.1575 ± 0.0331 ± 0.0003
0.450 − 0.500 GeV/c	0.2796 ± 0.0343 ± 0.0019	0.1894 ± 0.0348 ± 0.0003
0.500 − 0.550 GeV/c	0.3021 ± 0.0330 ± 0.0023	0.1284 ± 0.0317 ± 0.0003
0.550 − 0.600 GeV/c	0.3474 ± 0.0345 ± 0.0028	0.1593 ± 0.0334 ± 0.0004
0.600 − 0.650 GeV/c	0.3849 ± 0.0338 ± 0.0032	0.1387 ± 0.0312 ± 0.0004
0.650 − 0.700 GeV/c	0.3624 ± 0.0332 ± 0.0067	0.1309 ± 0.0313 ± 0.0022
0.700 − 0.750 GeV/c	0.3878 ± 0.0328 ± 0.0033	0.1079 ± 0.0296 ± 0.0005
0.750 − 0.800 GeV/c	0.3617 ± 0.0315 ± 0.0032	0.1064 ± 0.0278 ± 0.0005
0.800 − 0.900 GeV/c	0.3494 ± 0.0224 ± 0.0068	0.1135 ± 0.0207 ± 0.0021
0.900 − 1.000 GeV/c	0.2794 ± 0.0222 ± 0.0065	0.1309 ± 0.0222 ± 0.0029
1.000 − 1.100 GeV/c	0.2684 ± 0.0210 ± 0.0188	0.1026 ± 0.0208 ± 0.0072
1.100 − 1.200 GeV/c	0.2302 ± 0.0204 ± 0.0286	0.0976 ± 0.0209 ± 0.0121
1.200 − 1.300 GeV/c	0.1576 ± 0.0199 ± 0.0306	0.0972 ± 0.0220 ± 0.0189
1.300 − 1.400 GeV/c	0.1720 ± 0.0184 ± 0.0356	0.0540 ± 0.0194 ± 0.0112
1.400 − 1.500 GeV/c	0.1168 ± 0.0199 ± 0.0256	0.0778 ± 0.0229 ± 0.0171
1.500 − 1.600 GeV/c	0.0795 ± 0.0227 ± 0.0232	0.0942 ± 0.0284 ± 0.0274
1.600 − 1.700 GeV/c	0.0834 ± 0.0212 ± 0.0266	0.0417 ± 0.0254 ± 0.0133
1.700 − 1.800 GeV/c	0.0225 ± 0.0266 ± 0.0055	0.1134 ± 0.0350 ± 0.0255
1.800 − 1.900 GeV/c	0.0925 ± 0.0286 ± 0.0670	0.0260 ± 0.0383 ± 0.0188
1.900 − 2.000 GeV/c	0.0256 ± 0.0298 ± 0.0069	0.0640 ± 0.0408 ± 0.0168
2.000 − 2.100 GeV/c	0.0681 ± 0.0203 ± 0.1946	$0.0000\,{}^{+0.0180}_{-0.0000}\pm 0.0107$
2.100 − 2.200 GeV/c	0.0323 ± 0.0263 ± 0.0102	0.0210 ± 0.0340 ± 0.0066
2.200 − 2.300 GeV/c	0.0176 ± 0.0295 ± 0.0026	0.0653 ± 0.0405 ± 0.0070
2.300 − 2.400 GeV/c	$0.0000\,{}^{+0.0312}_{-0.0000}\pm 0.0251$	0.0506 ± 0.0322 ± 0.0024

events, as well as the bias induced by cutting away preferentially low-multiplicity events.

In order to be able to compare with other experiments, in Figs. 6 and 7 we show also the total amount of pions and protons, including K_s^0 and Λ decay products. The error bars in all figures correspond to statistical and momentum dependent systematical errors added in quadrature. The latter include the uncertainty of the dE/dx and TOF parametrization for the
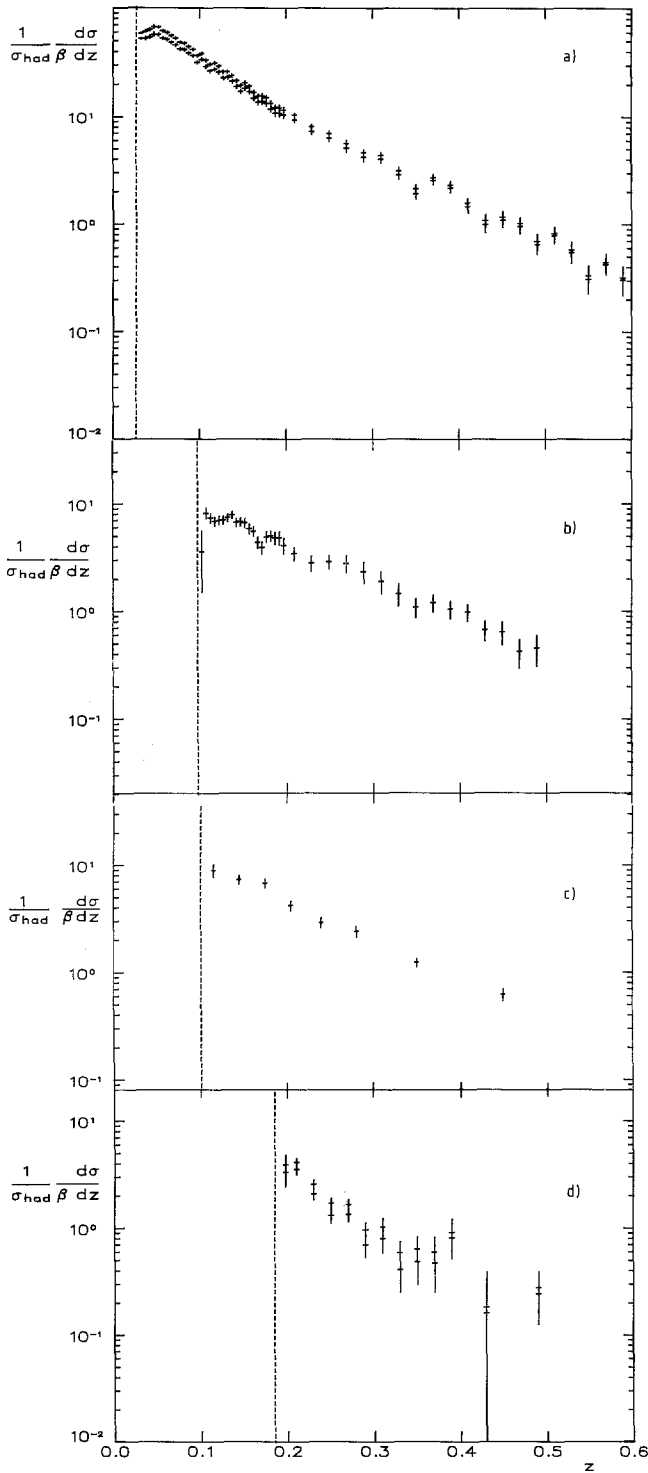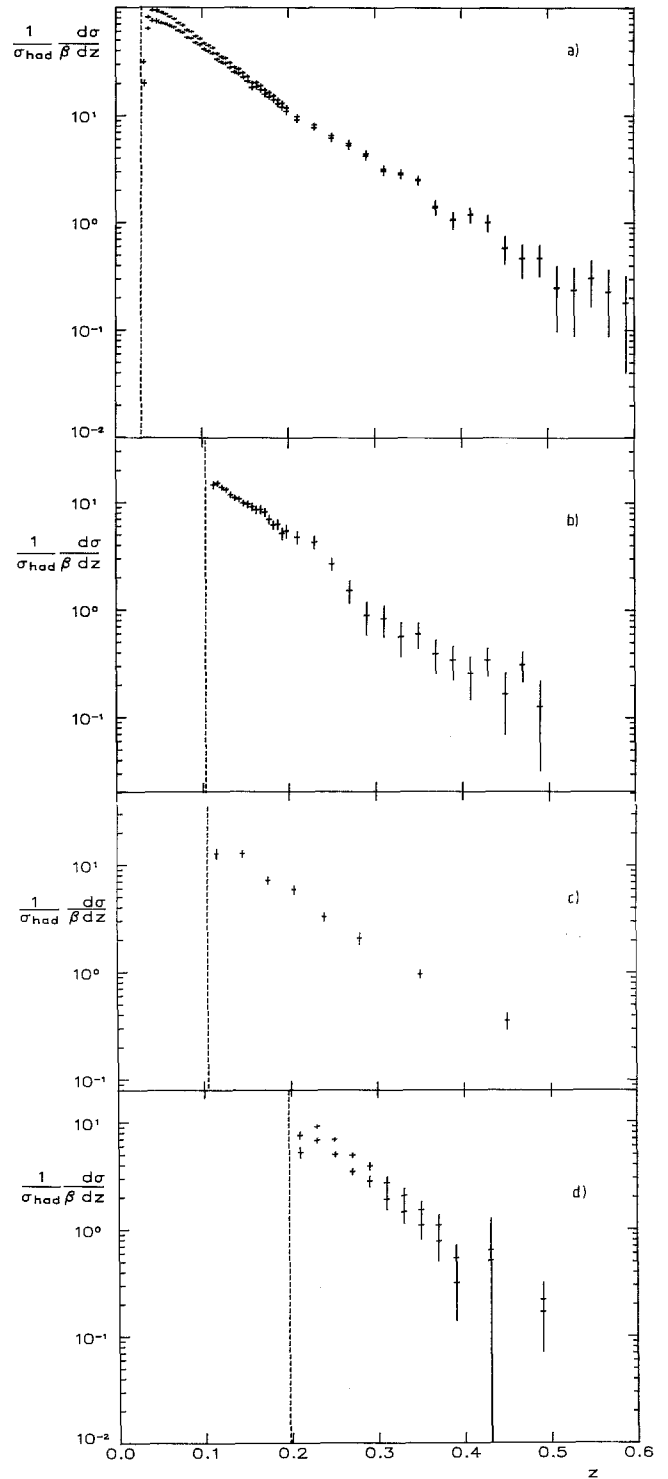
charged particles, and of our Monte Carlo simulation; for the direct $\Upsilon(1S)$ data an important portion of the systematic uncertainty comes from the errors on the constants needed to determine a, a', a'' for the continuum subtraction. A momentum independent overall uncertainty, which amounts to $\pm 1.8\%$ in all charged particles histograms and 3.6% in the K^0 histograms is not included in the error bars. The latter is determined by the uncertainty in the vertex finding efficiency, which has been investigated by varying the cut on the distance of the K_s^0 vertex from the interaction point.

Average multiplicities for all hadrons have been obtained by integrating the momentum distributions of Fig. 5. The results are compared to the Lund Monte Carlo predictions and to other experiments in Table 9. The systematic errors include the uncertainty of the extrapolation to the full momentum range. To illustrate the contribution from K_s^0 and Λ decays to inclusive pion and proton production, we have given the numbers corrected in both ways: with all decay products of these particles removed and included.

The most striking difference between quark and gluon fragmentation data is the enhancement of proton production in the Υ decays. This has first been observed by DASP II [1], and later confirmed by CLEO [2]. Surprisingly, the enhancement of direct protons (1.7 ± 0.2) is considerably smaller than that for Λ (2.5 ± 0.2) or other hyperons [2, 3].

Fig. 6a–d. Normalized scaling cross section for inclusive $\pi^{\pm}$ **a**, $K^{\pm}$ **b**, $K^0/\bar{K}^0$ **c** and $2\times$ cross section for inclusive $\bar{p}$ **d** production in $e^+e^- \to$ hadrons at 9.98 GeV. The dashed lines mark the kinematical limit. The upper points in **a** include pions from K_s^0 and Λ decays, the upper points in **d** include $\bar{p}$ from $\bar{\Lambda}$ decays

Fig. 7a–d. Normalized scaling cross section for inclusive $\pi^{\pm}$ **a**, $K^{\pm}$ **b**, $K^0/\bar{K}^0$ **c** and $2\times$ cross section for inclusive $\bar{p}$ **d** production in direct $\Upsilon(1S)$ decays. The dashed lines mark the kinematical limit. The upper points in **a** include pions from K_s^0 and Λ decays, the upper points in **d** include $\bar{p}$ from $\bar{\Lambda}$ decays

Table 5. $\dfrac{1}{\sigma_{\text{had}}}\dfrac{d\sigma(\pi^{\pm})}{\beta\,dz}$ of direct $\Upsilon(1S)$ decays and of $e^{+}e^{-}$-annihilation at 9.98 GeV. An overall uncertainty of $\pm1.8\%$ is not included in the systematic errors

z interval	$\Upsilon(1S)_{\text{dir}}$	continuum at 9.98 GeV
0.030 — 0.035	19.82 ± 0.81 ± 1.12	52.03 ± 0.99 ± 0.13
0.035 — 0.040	63.60 ± 1.28 ± 1.26	52.34 ± 1.61 ± 0.91
0.040 — 0.045	75.22 ± 1.46 ± 2.12	53.82 ± 1.50 ± 1.44
0.045 — 0.050	74.35 ± 1.43 ± 2.75	57.24 ± 1.51 ± 2.06
0.050 — 0.055	71.45 ± 1.39 ± 1.15	56.66 ± 1.49 ± 0.77
0.055 — 0.060	70.04 ± 1.30 ± 0.64	52.60 ± 1.40 ± 0.18
0.060 — 0.065	67.42 ± 1.27 ± 0.63	51.07 ± 1.35 ± 0.21
0.065 — 0.070	65.19 ± 1.22 ± 0.66	48.13 ± 1.30 ± 0.29
0.070 — 0.075	60.56 ± 1.16 ± 0.58	45.57 ± 1.26 ± 0.23
0.075 — 0.080	58.41 ± 1.12 ± 0.59	41.91 ± 1.18 ± 0.26
0.080 — 0.085	52.64 ± 1.08 ± 0.51	41.39 ± 1.17 ± 0.23
0.085 — 0.090	51.72 ± 1.04 ± 0.51	38.49 ± 1.13 ± 0.24
0.090 — 0.095	47.10 ± 0.99 ± 0.43	36.49 ± 1.04 ± 0.19
0.095 — 0.100	45.09 ± 0.94 ± 0.40	31.62 ± 0.98 ± 0.16
0.100 — 0.105	40.97 ± 0.93 ± 0.38	33.77 ± 1.00 ± 0.19
0.105 — 0.110	39.33 ± 0.89 ± 0.33	29.00 ± 0.93 ± 0.14
0.110 — 0.115	37.37 ± 0.85 ± 0.30	26.51 ± 0.89 ± 0.12
0.115 — 0.120	33.03 ± 0.80 ± 0.27	27.19 ± 0.89 ± 0.13
0.120 — 0.125	31.18 ± 0.78 ± 0.25	25.65 ± 0.87 ± 0.13
0.125 — 0.130	30.12 ± 0.74 ± 0.23	22.76 ± 0.83 ± 0.11
0.130 — 0.135	27.44 ± 0.73 ± 0.22	23.01 ± 0.82 ± 0.13
0.135 — 0.140	25.09 ± 0.70 ± 0.23	21.27 ± 0.80 ± 0.16
0.140 — 0.145	24.30 ± 0.67 ± 0.26	18.97 ± 0.76 ± 0.18
0.145 — 0.150	22.42 ± 0.64 ± 0.26	17.10 ± 0.72 ± 0.18
0.150 — 0.155	20.71 ± 0.65 ± 0.27	18.38 ± 0.74 ± 0.23
0.155 — 0.160	18.08 ± 0.62 ± 0.29	17.02 ± 0.73 ± 0.26
0.160 — 0.165	18.32 ± 0.60 ± 0.37	14.84 ± 0.69 ± 0.29
0.165 — 0.170	17.26 ± 0.58 ± 0.40	13.63 ± 0.67 ± 0.32
0.170 — 0.175	15.67 ± 0.58 ± 0.42	13.86 ± 0.69 ± 0.37
0.175 — 0.180	14.87 ± 0.58 ± 0.42	13.33 ± 0.68 ± 0.37
0.180 — 0.185	13.91 ± 0.56 ± 0.41	11.80 ± 0.66 ± 0.35
0.185 — 0.190	12.76 ± 0.54 ± 0.39	10.80 ± 0.64 ± 0.33
0.190 — 0.195	11.92 ± 0.56 ± 0.38	10.78 ± 0.68 ± 0.34
0.195 — 0.200	10.87 ± 0.54 ± 0.34	10.35 ± 0.65 ± 0.33
0.200 — 0.220	9.04 ± 0.28 ± 0.29	9.32 ± 0.34 ± 0.29
0.220 — 0.240	7.58 ± 0.29 ± 0.19	7.23 ± 0.37 ± 0.17
0.240 — 0.260	6.06 ± 0.29 ± 0.21	6.26 ± 0.36 ± 0.21
0.260 — 0.280	5.20 ± 0.27 ± 0.28	5.06 ± 0.32 ± 0.26
0.280 — 0.300	4.16 ± 0.23 ± 0.25	4.18 ± 0.29 ± 0.24
0.300 — 0.320	3.01 ± 0.20 ± 0.15	4.03 ± 0.26 ± 0.16
0.320 — 0.340	2.78 ± 0.18 ± 0.14	2.85 ± 0.22 ± 0.10
0.340 — 0.360	2.44 ± 0.16 ± 0.13	1.91 ± 0.20 ± 0.07
0.360 — 0.380	1.37 ± 0.15 ± 0.12	2.55 ± 0.20 ± 0.08
0.380 — 0.400	1.05 ± 0.14 ± 0.12	2.16 ± 0.19 ± 0.07
0.400 — 0.420	1.18 ± 0.13 ± 0.13	1.45 ± 0.17 ± 0.07
0.420 — 0.440	0.99 ± 0.11 ± 0.12	0.99 ± 0.15 ± 0.04
0.440 — 0.460	0.57 ± 0.11 ± 0.12	1.08 ± 0.15 ± 0.05
0.460 — 0.480	0.46 ± 0.10 ± 0.12	0.95 ± 0.13 ± 0.04
0.480 — 0.500	0.46 ± 0.08 ± 0.12	0.64 ± 0.12 ± 0.03
0.500 — 0.520	0.25 ± 0.08 ± 0.12	0.78 ± 0.11 ± 0.04
0.520 — 0.540	0.23 ± 0.07 ± 0.13	0.54 ± 0.10 ± 0.03
0.540 — 0.560	0.30 ± 0.06 ± 0.13	0.31 ± 0.08 ± 0.02
0.560 — 0.580	0.23 ± 0.06 ± 0.13	0.42 ± 0.09 ± 0.02
0.580 — 0.600	0.18 ± 0.05 ± 0.13	0.30 ± 0.08 ± 0.03

Table 6. $\dfrac{1}{\sigma_{\text{had}}}\dfrac{d\sigma(K^{\pm})}{\beta\,dz}$ of direct $\Upsilon(1S)$ decays and of $e^{+}e^{-}$-annihilation at 9.98 GeV. An overall uncertainty of $\pm1.8\%$ is not included in the systematic errors

z interval	$\Upsilon(1S)_{\text{dir}}$	continuum at 9.98 GeV
0.100 — 0.105		3.55 ± 2.05 ± 0.04
0.105 — 0.110		8.20 ± 0.96 ± 0.02
0.110 — 0.115	14.59 ± 1.03 ± 0.10	7.33 ± 0.76 ± 0.01
0.115 — 0.120	15.12 ± 0.78 ± 0.12	6.83 ± 0.66 ± 0.02
0.120 — 0.125	13.83 ± 0.68 ± 0.11	6.92 ± 0.63 ± 0.02
0.125 — 0.130	13.14 ± 0.64 ± 0.11	7.00 ± 0.61 ± 0.03
0.130 — 0.135	11.69 ± 0.60 ± 0.12	7.40 ± 0.61 ± 0.05
0.135 — 0.140	10.99 ± 0.57 ± 0.13	7.85 ± 0.62 ± 0.07
0.140 — 0.145	10.69 ± 0.54 ± 0.18	6.68 ± 0.55 ± 0.10
0.145 — 0.150	9.84 ± 0.52 ± 0.30	6.78 ± 0.57 ± 0.20
0.150 — 0.155	9.57 ± 0.50 ± 0.43	6.60 ± 0.57 ± 0.29
0.155 — 0.160	9.07 ± 0.48 ± 0.53	5.81 ± 0.53 ± 0.33
0.160 — 0.165	8.55 ± 0.47 ± 0.44	5.50 ± 0.50 ± 0.28
0.165 — 0.170	8.57 ± 0.47 ± 0.55	4.33 ± 0.45 ± 0.28
0.170 — 0.175	8.10 ± 0.44 ± 0.50	3.89 ± 0.44 ± 0.24
0.175 — 0.180	6.95 ± 0.45 ± 0.39	4.91 ± 0.48 ± 0.28
0.180 — 0.185	6.16 ± 0.43 ± 0.31	5.01 ± 0.49 ± 0.25
0.185 — 0.190	6.24 ± 0.43 ± 0.48	4.79 ± 0.50 ± 0.37
0.190 — 0.195	5.14 ± 0.44 ± 0.46	4.79 ± 0.51 ± 0.43
0.195 — 0.200	5.41 ± 0.44 ± 0.54	4.05 ± 0.52 ± 0.41
0.200 — 0.220	4.75 ± 0.22 ± 0.58	3.43 ± 0.26 ± 0.42
0.220 — 0.240	4.27 ± 0.26 ± 0.51	2.78 ± 0.31 ± 0.33
0.240 — 0.260	2.67 ± 0.30 ± 0.16	2.87 ± 0.37 ± 0.17
0.260 — 0.280	1.50 ± 0.29 ± 0.19	2.76 ± 0.35 ± 0.36
0.280 — 0.300	0.89 ± 0.25 ± 0.16	2.31 ± 0.31 ± 0.41
0.300 — 0.320	0.83 ± 0.21 ± 0.16	1.89 ± 0.25 ± 0.36
0.320 — 0.340	0.56 ± 0.17 ± 0.11	1.44 ± 0.20 ± 0.27
0.340 — 0.360	0.60 ± 0.13 ± 0.08	1.08 ± 0.16 ± 0.15
0.360 — 0.380	0.39 ± 0.12 ± 0.05	1.19 ± 0.15 ± 0.16
0.380 — 0.400	0.34 ± 0.11 ± 0.05	1.04 ± 0.14 ± 0.14
0.400 — 0.420	0.26 ± 0.10 ± 0.03	0.98 ± 0.13 ± 0.11
0.420 — 0.440	0.34 ± 0.09 ± 0.04	0.66 ± 0.12 ± 0.08
0.440 — 0.460	0.16 ± 0.09 ± 0.03	0.64 ± 0.13 ± 0.09
0.460 — 0.480	0.31 ± 0.08 ± 0.06	0.42 ± 0.10 ± 0.07
0.480 — 0.500	0.13 ± 0.09 ± 0.02	0.45 ± 0.13 ± 0.06

Table 7. $\dfrac{1}{\sigma_{\text{had}}}\dfrac{d\sigma(K^{0}/\bar{K}^{0})}{\beta\,dz}$ of direct $\Upsilon(1S)$ decays and of $e^{+}e^{-}$-annihilation at 9.98 GeV. An overall systematic uncertainty of $\pm3.6\%$ has to be added

z interval	$\Upsilon(1S)_{\text{dir}}$	continuum at 9.98 GeV
0.100 — 0.130		8.90 ± 1.19
0.105 — 0.130	12.75 ± 1.36	
0.130 — 0.160	12.73 ± 0.91	7.30 ± 0.70
0.160 — 0.190	7.13 ± 0.55	6.75 ± 0.66
0.190 — 0.220	5.86 ± 0.52	4.18 ± 0.44
0.220 — 0.260	3.26 ± 0.29	2.88 ± 0.31
0.260 — 0.300	2.07 ± 0.26	2.38 ± 0.27
0.300 — 0.400	0.957 ± 0.082	1.23 ± 0.11
0.400 — 0.500	0.354 ± 0.060	0.618 ± 0.079

The most successful theoretical descriptions of quark and gluon fragmentation come from string fragmentation [13] and parton shower [14] models. Although there is rough overall agreement, the Lund Monte Carlo cannot describe the details of the distributions. The ratio of protons from direct $\Upsilon(1S)$ decays and $q\bar{q}$ jets is slightly overestimated, whereas the corresponding ratio for lambda hyperons is significantly underestimated [3]. Pion and kaon production is described only approximately, although the origin of the differences is more difficult to determine, since charm decays likely play an important role for stable meson production in $q\bar{q}$ events. New efforts will be necessary in order to achieve a more realistic description of quark and gluon fragmentation.

Table 8. $2\cdot\dfrac{1}{\sigma_{\text{had}}}\dfrac{d\sigma(\bar{p})}{\beta\,dz}$ of direct $\Upsilon(1S)$ decays and of $e^{+}e^{-}$-annihilation at 9.98 GeV. An overall uncertainty of $\pm1.8\%$ is not included in the systematic errors

z interval	$\Upsilon(1S)_{\text{dir}}$	continuum at 9.98 GeV
0.195 — 0.200		3.294 ± 0.897 ± 0.009
0.200 — 0.220	5.184 ± 0.561 ± 0.064	3.502 ± 0.372 ± 0.009
0.220 — 0.240	6.736 ± 0.301 ± 0.112	2.045 ± 0.253 ± 0.027
0.240 — 0.260	4.950 ± 0.228 ± 0.078	1.298 ± 0.192 ± 0.017
0.260 — 0.280	3.426 ± 0.197 ± 0.108	1.331 ± 0.187 ± 0.040
0.280 — 0.300	2.786 ± 0.163 ± 0.273	0.691 ± 0.147 ± 0.068
0.300 — 0.320	1.891 ± 0.148 ± 0.341	0.794 ± 0.154 ± 0.143
0.320 — 0.340	1.447 ± 0.130 ± 0.300	0.405 ± 0.133 ± 0.084
0.340 — 0.360	1.082 ± 0.129 ± 0.255	0.483 ± 0.149 ± 0.114
0.360 — 0.380	0.771 ± 0.138 ± 0.233	0.468 ± 0.169 ± 0.141
0.380 — 0.400	0.313 ± 0.152 ± 0.085	0.808 ± 0.203 ± 0.216
0.400 — 0.460	0.511 ± 0.089 ± 0.609	0.158 ± 0.081 ± 0.188
0.460 — 0.520	0.168 ± 0.087 ± 0.042	0.240 ± 0.113 ± 0.026

Table 9. $\pi^{\pm}$, $K^{\pm}$, $K^0/\bar{K}^0$ and $2 \cdot \bar{p}$ multiplicities obtained with the ARGUS detector, compared to the LUND Monte Carlo (version 6.2, [9]) and to results from other experiments. The continuum data are taken at 9.98 GeV (this experiment), in the range 9.4 to 10.1 GeV (DASP II) and at 10.49 GeV (CLEO), respectively. Contributions from K_s^0 and Λ to these multiplicities are determined from experimental data

		$\Upsilon(1S)_{dir}$	continuum
$\pi^{\pm}$	(not from K_s^0, Λ) this expt.	$6.691 \pm 0.029 \pm 0.123$	$5.694 \pm 0.034 \pm 0.103$
	(incl. K_s^0, Λ) this expt.	7.55 ± 0.14	6.38 ± 0.12
	(not from K_s^0, Λ) Lund	6.912 ± 0.003	5.676 ± 0.002
	DASP II [1]	6.1 ± 0.6	5.5 ± 0.6
	CLEO [2]	8.7 ± 0.4	8.3 ± 0.4
$K^0/\bar{K}^0$	this expt.	$1.033 \pm 0.036 \pm 0.037$	$0.910 \pm 0.050 \pm 0.034$
	LUND	0.809 ± 0.001	0.907 ± 0.001
	CLEO [2]	1.05 ± 0.13	0.92 ± 0.12
$K^{\pm}$	this expt.	$0.908 \pm 0.016 \pm 0.020$	$0.888 \pm 0.018 \pm 0.024$
	LUND	0.828 ± 0.001	0.948 ± 0.001
	DASP II [1]	1.22 ± 0.23	1.26 ± 0.29
	CLEO [2]	1.4 ± 0.2	1.3 ± 0.2
$2 \cdot \bar{p}$	(not from $\bar{\Lambda}$) this expt.	$0.361 \pm 0.011 \pm 0.023$	$0.212 \pm 0.012 \pm 0.012$
	(incl. $\bar{\Lambda}$) this expt.	0.507 ± 0.028	0.271 ± 0.018
	(not from $\bar{\Lambda}$) Lund	0.491 ± 0.001	0.254 ± 0.001
	DASP II [1]	0.64 ± 0.17	0.10 ± 0.04
	CLEO [2]	0.60 ± 0.09	0.40 ± 0.06

References

1. H. Albrecht et al. (DASP II): Phys. Lett. 102 B (1981) 291
2. S. Behrends et al. (CLEO): Phys. Rev. D 31 (1985) 2161
3. H. Albrecht et al. (ARGUS): Z. Phys. C – Particles and Fields 39 (1988) 177
4. see e.g. G. Schierholz, M. Teper: Z. Phys. C – Particles and Fields 13 (1982) 53; B. Andersson et al.: Phys. Scr. 32 (1985) 574
5. H. Albrecht et al. (ARGUS): Nucl. Instrum. Methods A 275 (1989) 1
6. M. Danilov et al.: Nucl. Instrum. Methods 217 (1983) 153
7. R. Heller et al.: Nucl. Instrum. Methods A 235 (1985) 26
8. W. Funk: Diplomarbeit, IHEP-HD/88-3, Heidelberg 1988
9. T. Sjöstrand: Comp. Phys. Commun. 27 (1982) 243; 39 (1986) 347
10. S. Werner: Diplomarbeit, IHEP-HD/87-1, Heidelberg 1987
11. F.A. Berends, R. Kleiss: Nucl. Phys. B 178 (1981) 141
12. H. Gennow: Internal Report DESY F15-85-02
13. B. Andersson et al.: Phys. Rep. 97 (1983) 31 and references therein
14. R.D. Field, S. Wolfram: Nucl. Phys. B 213 (1983) 65; G. Marchesini, B.R. Webber: Nucl. Phys. B 238 (1984) 1; B.R. Webber: Nucl. Phys. B 238 (1984) 492